Journal of Alloys and Compounds 506 (2010) 446–455

Contents lists available at ScienceDirect

Journal of Alloys and Compounds

journal homepage: www.elsevier.com/locate/jallcom

# Template-free synthesis, characterization, growth mechanism and photoluminescence property of $Eu(OH)_3$ and $Eu_2O_3$ nanospindles

Dengsong Zhang[a], Tingting Yan[a], Liyi Shi[a,*], Hongrui Li[a], Joseph F. Chiang[b,**]

[a] Research Center of Nano Science and Technology, Shanghai University, Shanghai 200444, China
[b] Department of Chemistry and Biochemistry, State University of New York at Oneonta, 100 Ravine Parkway, Oneonta, NY, 13820, USA

ARTICLE INFO

*Article history:*
Received 27 April 2010
Received in revised form 1 July 2010
Accepted 6 July 2010
Available online 14 July 2010

*Keywords:*
Europium oxide
Nanostructures
Photoluminescence

ABSTRACT

A simple aqueous solution route was introduced for the fabrication of uniform $Eu(OH)_3$ and $Eu_2O_3$ nanospindles, nanorods and nanobundles by using $Eu(NO_3)_3$ and NaOH as the starting reaction reagents at room temperature and atmosphere pressure without any surfactant and template. The influence of the molar ratios of $[OH^-]/[Eu^{3+}]$, reaction time, and temperature was investigated. It is demonstrated that the size of $Eu(OH)_3$ nanospindle can be well tuned by adjusting the $[Eu^{3+}]/[OH^-]$ molar ratios. The possible growth mechanism of $Eu(OH)_3$ and $Eu_2O_3$ nanostructures is also discussed. The room-temperature photoluminescence analysis shows that $Eu_2O_3$ nanostructures have an intensive emission peak of $Eu^{3+}$ ion at around 611 nm due to the $^5D_0$–$^7F_2$ forced electric dipole transition of $Eu^{3+}$ ions. It is found that the relative peak intensity increases with increasing reaction time.



## 1. Introduction

Nanostructured materials have been documented with excellent properties in optics, electronics, magnetism, and catalysis as compared with their bulk counterpart due to their low dimensionality [1–3]. In recent years, size control, crystallization, and morphology of inorganic materials have attracted enormous attention in material research fields, which is of great importance for the development of new functional devices [4,5]. Those nanostructured materials have been used as building blocks to successfully fabricate functional microdevices [2,6].

Rare earth metal oxides have been widely applied in various fields, such as high-performance luminescence devices, biochemical applications, catalysts and other functional materials, due to the electronic, optical and chemical characteristics arising from the electron transitions within the 4f shell [7–11]. The luminescence of $Eu^{3+}$ is important and interesting because the major emission band at ~611 nm (red) is one of the three primary colors [11]. Therefore, in many host lattices, $Eu^{3+}$ has been studied intensively as a luminescence activator, which is used widely in fluorescent lamps, projection television tubes, field emission plays and cathode-ray tubes [12–17]. In recent years, $Eu_2O_3$ nanostructures have received a tremendous amount of attention as they have a higher packing density and a larger percentage of active sites compared with bulk materials [18]. Various $Eu_2O_3$ nanostructures, including, nanorods, nanotubes, nanospheres and nanowires, have also received a great amount of attention [19–24]. However, to the best of our knowledge, there are few reports on the synthesis of $Eu_2O_3$ nanospindles, except that Wang et al. reported the synthesis of mesoporous $Eu_2O_3$ microspindles via a polyethylene glycol assisted reflux method [25]. Most recently, Xu et al. reported a simple method to synthesize the submicrospindles at 5 °C [26]. However, the synthetic strategy operating at this low temperature is also an energy-consuming route and a long aging time of 5 days is inevitably required. It is noted that the spindle-like nanocrystals with nanometer or micrometer size have been reported in recent years such as $PbWO_4$ [27], $LnVO_4$ (Ln = La, Ce, Pr, Nd, Sm, Eu, Gd, Tb, Dy, Ho, Er, Tm, Yb, Lu) [28], $CeO_2$ [29], $YF_3$:$Eu^{3+}$ [5], $CePO_4$:$Tb^{3+}$ [30], $LnPO_4$ [31], α-$Ga_2O_3$, and β-$Ga_2O_3$ [32]. Most of these synthetic routes are complicated, energy-consuming and/or require surfactants and templates. The removal of the surfactant is still a problem because of the strong force between the reagent and favorable crystal surfaces, which produces impurities and is not environmentally benign. Moreover, it is obvious that the complexity and cost will increase mostly when a large-scale synthesis of uniform nanostructures is needed. The room temperature (R.T.) and ambient pressure in aqueous solution method without using templates or other additives have been considered as one of the most promising routes because it is a green chemical approach of practical significance [33]. So it is still very significant to develop a simple approach for large-scale synthesis of $Eu(OH)_3$ and $Eu_2O_3$ nanostructured without the assistance of any added surfactant, catalyst or template under an ambient temperature.

* Corresponding author.
** Corresponding author. Tel.: +1 607 436 3181; fax: +1 607 436 2654.
*E-mail addresses:* shiliyi@shu.edu.cn (L. Shi), chiangjf@oneonta.edu (J.F. Chiang).

0925-8388/$ – see front matter © 2010 Elsevier B.V. All rights reserved.
doi:10.1016/j.jallcom.2010.07.026

Previously, we have synthesized $Eu_2O_3$ nanotubes, nanowires and carbon nanotube/$Eu(OH)_3$ core–shell nanowires by a carbon nanotube assisted solvothermal method [7] and a surfactant assisted reflux method [34]. Most recently, we have synthesized $Eu_2O_3$ nanorods by a precipitation method at 60 °C [35]. Herein, we report a facile method to synthesize the highly uniform and single-crystalline $Eu(OH)_3$ nanospindles (R.T. and ambient pressure.) in aqueous solution with ordinary and inexpensive inorganic reagents and without using any template or surfactant. The simplicity of this process, low cost, and availability of raw materials would favor scaled-up industrial manufacturing.

## 2. Experimental procedures

Analytical grade NaOH and $Eu(NO_3)_3{\cdot}6H_2O$ were purchased from Sinopharm Chemical Regent Company and were used without further purification. Deionized water was used throughout the process.

In a typical synthetic procedure, $Eu(NO_3)_3$ solution (0.2 mol/L) was added to into NaOH solution (16 mol/L) under high speed magnetic stirring. The suspension was maintained at R.T. for 12 h. The precipitate was collected by centrifuging and washed repeatedly with deionized water. It was then dried in an oven at 80 °C for 3 h. The oxide phosphor was obtained by calcinations in air at a heating rate of 5 °C/min from R.T. to 600 °C. Then the temperature was maintained at 600 °C for 4 h.

The powder X-ray diffraction (XRD) measurements were performed with Rigaku D/MAX-RB X-ray diffractometer by using Cu Kα (40 kV, 40 mA) radiation and a secondary beam graphite monochromator. The morphologies were observed by transmission electron microscopy (TEM, JEOL JEM-200CX), high-resolution transmission electron microscopy (HRTEM) (JEOL 3010 ARP) microscope and powdered samples were dispersed in ethanol by ultrasonication for 10 min in a KQ-250B ultrasonic bath. The morphologies were also examined by field emission scanning electron microscopy (SEM, JEOL JSM-6700F). Thermogravimetry and differential scanning calorimetry (TG–DSC) of the samples was carried out with a Netzsch STA 409 PC analyzer at a heating rate of 10 °C/min from R.T. to 1000 °C. The photoluminescence measurements were taken on a Cary-Eclipse 500 spectrofluorometer (VARIAN) with a 60 W Xenon lamp as an excitation source. The luminescence lifetime was measured with a Fluorolog-3 spectrofluorophotometer (JOBIN YVON Company, France) at R.T.

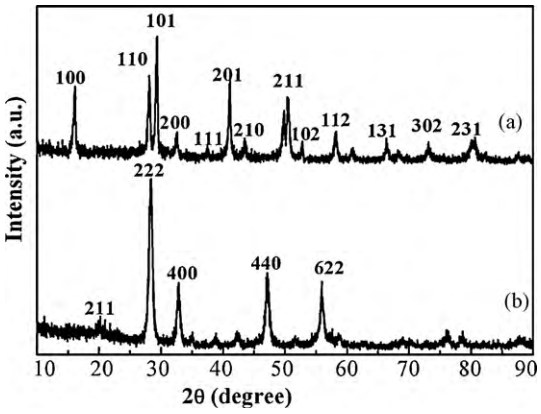


**Fig. 1.** XRD patterns of (a) $Eu(OH)_3$ and (b) $Eu_2O_3$ nanospindles.

## 3. Results and discussion

### 3.1. Characteristics of $Eu(OH)_3$ and $Eu_2O_3$ nanospindles

Fig. 1 shows the XRD patterns of $Eu(OH)_3$ and $Eu_2O_3$ nanospindles. All the diffraction peaks (Fig. 1a) can be indexed to a pure

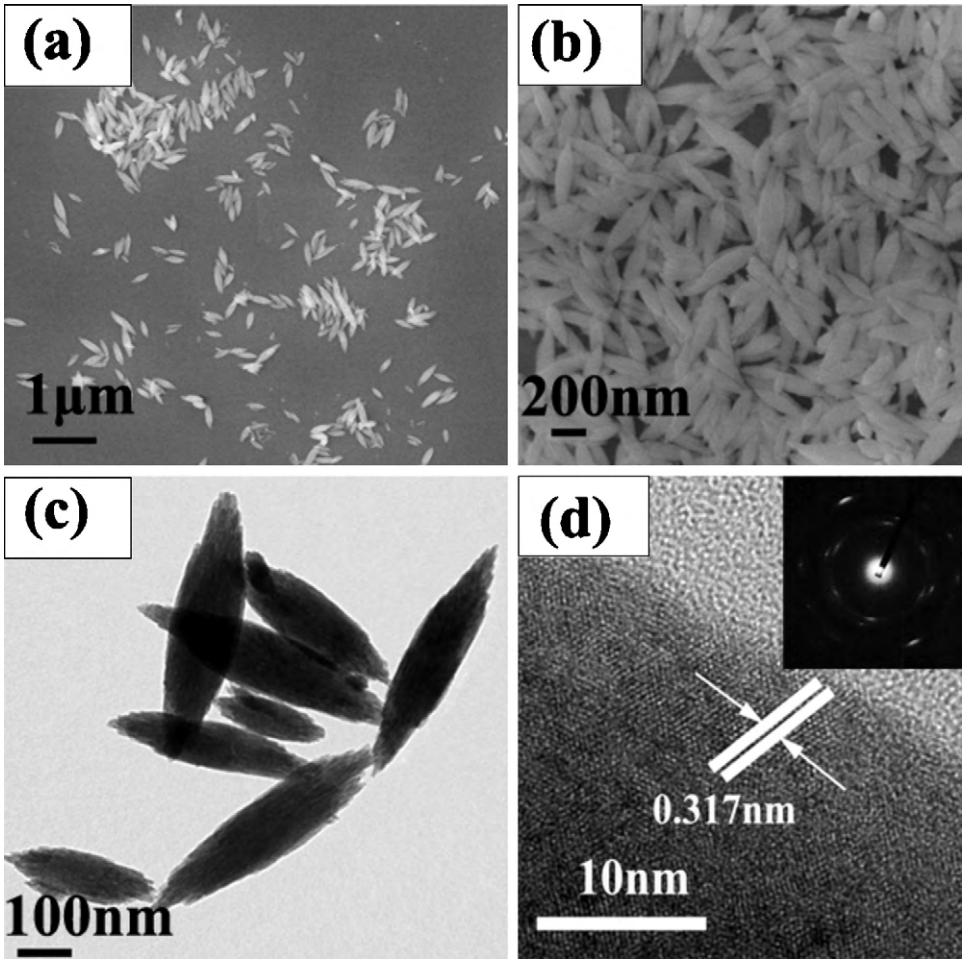


**Fig. 2.** (a and b) SEM images of $Eu(OH)_3$ nanospindles; (c) TEM, (d) HRTEM images and SAED pattern (inset of d) of $Eu(OH)_3$ nanospindles.

hexagonal phase of $Eu(OH)_3$ (JCPDS No. 17-0781). The ideal intensity ratio of a $Eu(OH)_3$ crystal between the (1 0 0) and (1 1 0) reflection approaches 1.2, while the measured ratio in this experiment is less than 0.97. This result may suggest that the present $Eu(OH)_3$ crystals may grow along the [1 1 0] axis, which has also been observed for some other one-dimensional (1D) materials [36]. Fig. 1b shows the XRD pattern of the products prepared by the subsequent calcinations of $Eu(OH)_3$ at 600 °C for 4 h. After calcinations, the diffraction peaks are observed at 20.0°, 28.4°, 32.9°, 47.3°, and 56.0°. These peaks correspond to the (2 1 1), (2 2 2), (4 0 0), (4 4 0), and (6 2 2) planes, which can be indexed to the pure body-centered cubic $Eu_2O_3$ (JCPDS No. 34-0392). It indicates that the cubic phase $Eu_2O_3$ has been produced.

The morphologies of the products have been examined by SEM, TEM and HRTEM. The SEM images of $Eu(OH)_3$ nanospindles (Fig. 2) are observed at different magnifications. From the low magnification image (Fig. 2a), the products are homogeneous and monodisperse. The medium SEM image (Fig. 2b) shows that the products are entirely comprised of nanospindles with a diameter of 80–160 nm and a length of 200–600 nm. No other morphologies are observed in the sample. The purity of nanospindles is as high as 90% (estimated from SEM images). It indicates that high-yield $Eu(OH)_3$ nanospindles can be easily prepared by this facile method. Moreover, as can be seen from TEM images (Fig. 2c), each spindle shows sharp-ends and curved edges. The width of these samples increases from the end to the center. The typical HRTEM image (Fig. 2d) of $Eu(OH)_3$ nanospindles clearly shows lattice fringes with

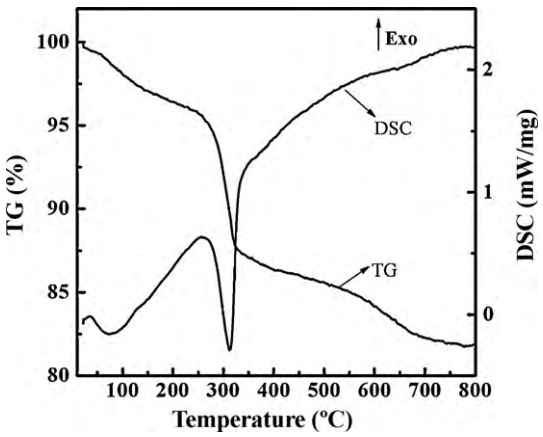


**Fig. 3.** TG–DSC curves of $Eu(OH)_3$ nanospindles.

interplanar spacing of 0.31 nm that corresponds to the (1 1 0) plane of $Eu(OH)_3$ phase, which implies the $Eu(OH)_3$ nanospindles grow along the [1 1 0] direction, and this result is in agreement with the XRD analysis presented in this work. The selected-area electron diffraction (SAED) pattern (inset in Fig. 2d) shows crystalline structure. The slightly elongated diffraction dots may attribute to lattice orientation imperfections among the primary particles prepared at R.T. [37]. It is noteworthy that SEM and TEM images were obtained from randomly selected areas of the sample and, as such,

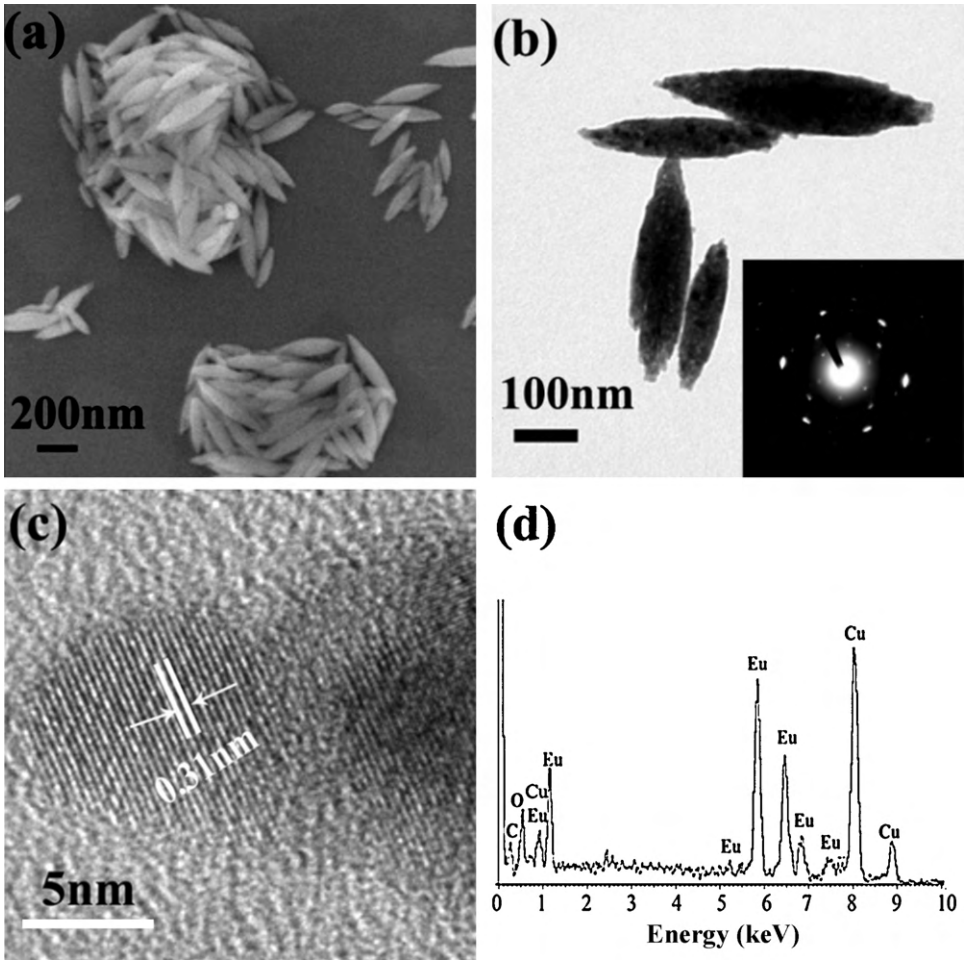


**Fig. 4.** (a) SEM image of $Eu_2O_3$ nanospindles; (b) TEM image and SAED pattern (inset) of $Eu_2O_3$ nanospindles; (c) HRTEM image of $Eu_2O_3$ nanospindles and (d) EDS pattern of $Eu_2O_3$ nanospindles.

are representative of the overall shapes and sizes of our as-prepared nanospindles.

The thermal behaviors of the $Eu(OH)_3$ sample are investigated with TG–DSC measurement, as shown in Fig. 3. It presents three stages of weight loss and the total weight loss is ~18.0%. The decomposition starts at ~50 °C and continues up to 600 °C. The first weight loss step (~4.4%) with an endothermic peak is at ~100 °C, which is attributed to the desorption of water molecules from the surface of the samples. The second decomposition occurred at ~312 °C with a sharp endothermic peak, owning to the decomposition of the $Eu(OH)_3$ and formation of EuOOH as shown in Eq. (1). The observed weight loss for the second step was about ~7.7% as compared with a theoretical weight loss of 8.9% for the conversion of $Eu(OH)_3$ to EuOOH. The weight loss observed in the last step is about 5.9% with a small endothermic process at around 420 °C, which is due to the conversion of EuOOH to $Eu_2O_3$ as shown in Eq. (2). The end products of TGA measurement are found to be pure $Eu_2O_3$, as inferred from XRD results. Those results are similar to the previous reports [35].

$$2Eu(OH)_3 \rightarrow 2EuOOH + 2H_2O \quad (1)$$

$$2EuOOH \rightarrow Eu_2O_3 + H_2O \quad (2)$$

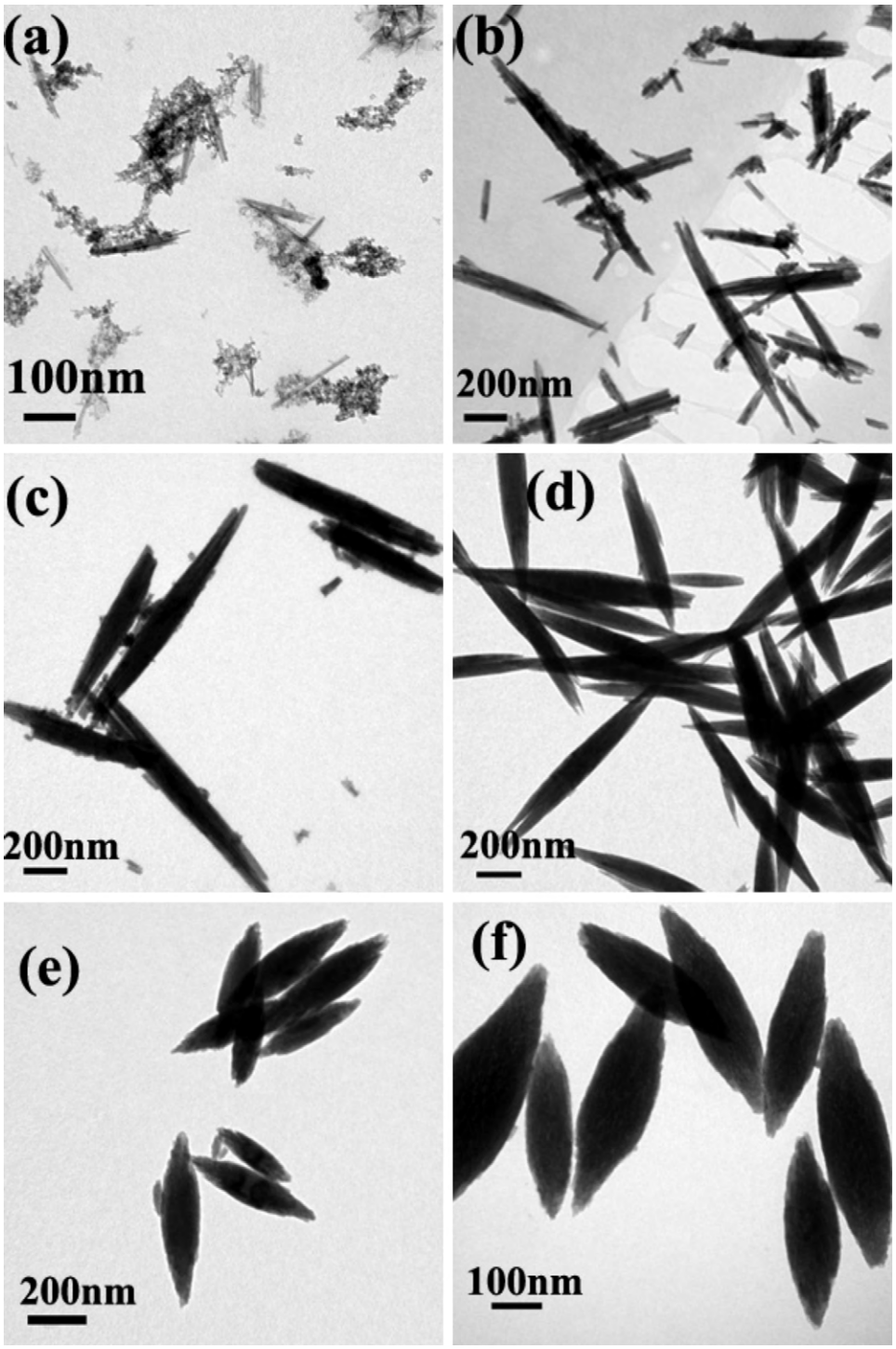


**Fig. 5.** TEM images of $Eu(OH)_3$ nanspindles prepared at R.T. under different $[OH^-]/[Eu^{3+}]$ molar ratios: (a) 15, (b) 25, (c) 50, (d) 100, (e) 240, and (f) 300.

On the basis of the TGA–DSC data, the $Eu(OH)_3$ samples are calcined at 600 °C in air to ensure their entire conversion into $Eu_2O_3$.

Fig. 4 shows the detail microscope image of $Eu_2O_3$ samples calcined at 600 °C for 4 h. It can be seen that the calcined samples (Fig. 4a) still maintain the spindle structure, which is similar to $Eu(OH)_3$ nanospindles. The products are entirely comprised of nanospindles (Fig. 4b) with a diameter of 80–120 nm and a length of 200–600 nm. The size of $Eu_2O_3$ nanospindles is smaller than that $Eu(OH)_3$ nanospindles as the density is higher than that of the precursor materials [26]. An SAED pattern (inset in Fig. 4b) from an individual nanospindle indicates that the $Eu_2O_3$ nanospindles are single crystalline. The corresponding SAED pattern indicates the (2 1 1), (4 0 0), (4 4 0) planes of $Eu_2O_3$ cubic phase, which is in agreement with the XRD results. The HRTEM image is shown in Fig. 4c. The well-resolved lattice fringes indicate that the spacing is about 0.31 nm corresponding to the (2 2 2) plane of the body-centered cubic $Eu_2O_3$. The EDS pattern (Fig. 4d) demonstrates the presence of O and Eu, and it is noted that the C and Cu peaks come from the Cu grids.

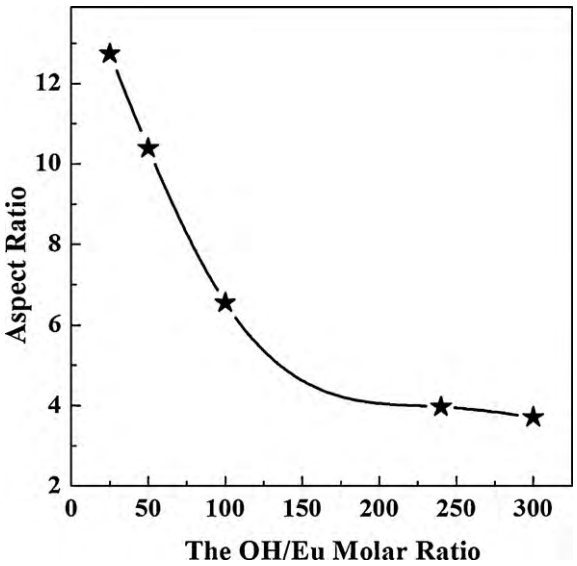


**Fig. 6.** Plots of aspect ratio against the molar ratios of $[OH^-]/[Eu^{3+}]$.

### 3.2. Synthesis factors and formation mechanism of $Eu(OH)_3$ nanostructures

In this process, it is found that the morphology and size of the products are greatly affected by the molar ratio of $[OH^-]/[Eu^{3+}]$, which can be confirmed by its dramatic effect on the morphologies of the products. In order to investigate the effect of $OH^-$ on the formation of size-controlled and uniform $Eu(OH)_3$ nanospindles in our synthetic method, the amount of NaOH was varied with the molar ratios of $[OH^-]/[Eu^{3+}]$ to be 15, 25, 50,100, 240, and 300 while the other conditions were kept unchanged (Fig. 5). The $Eu(OH)_3$ nanospindles could only be obtained under an optimized concentration of $OH^-$ ion. When the $[OH^-]/[Eu^{3+}]$ molar ratio is 10, the

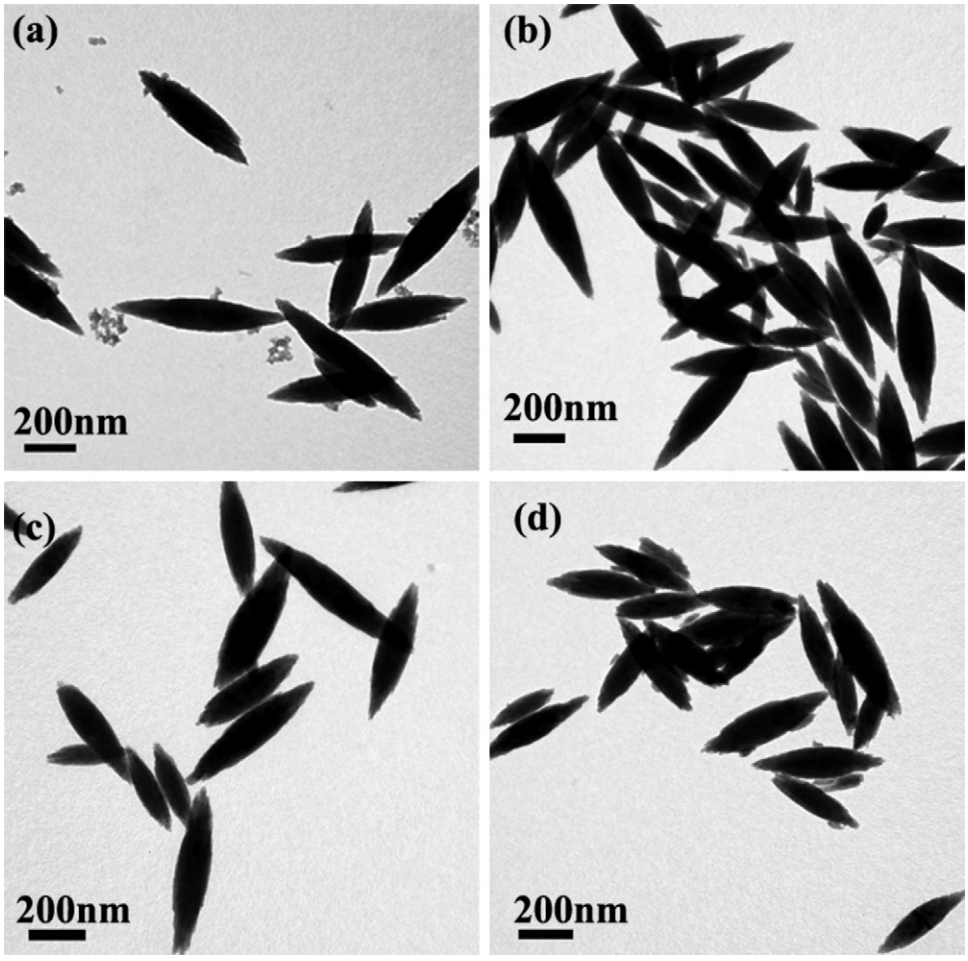


**Fig. 7.** TEM images of $Eu(OH)_3$ nanospindles prepared at R.T. for various aging times: (a) 10 min, (b) 1 h, (c) 6 h and (d) 72 h.

as-prepared samples are mainly comprised of aggregates of amorphous particles, coexisting with some nanorods. It is interesting to observe that some spindle-like nanoparticles are formed after an increasing $[OH^-]/[Eu^{3+}]$ molar ratio to 25. By careful observation, the surfaces of those spindles are rather rough and some amorphous particles are absorbed. When the $[OH^-]/[Eu^{3+}]$ molar ratio is increased to 50, the products are mostly composed of nanospindles. As increasing the $[OH^-]/[Eu^{3+}]$ molar ratio, more spindles will appear in the products at the expense of the amorphous particles, indicating that the structure is assembled from small nanoparticles and the size uniformity is greatly improved. When the $[OH^-]/[Eu^{3+}]$ molar ratio is increased to 100, the products are entirely composed of nanospindles with smooth surface. All the nanospindles are homogeneous, monodisperse and slimmer. In general, the $Eu(OH)_3$ nanospindles have an decreasing aspect ratio at higher $[OH^-]/[Eu^{3+}]$ molar ratio: average sizes are $1228 \times 96$ nm for 25:1, $825 \times 79$ nm for 50:1, $786 \times 120$ nm for 100:1, $471 \times 122$ nm for 240:1, and $427 \times 115$ nm for 300:1.The plots of aspect ratio of the nanospindles versus the $[OH^-]/[Eu^{3+}]$ molar ratios are presented in Fig. 6. As can be seen that the aspect ratio of $Eu(OH)_3$ nanospindles decreases with increasing the $[OH^-]/[Eu^{3+}]$ molar ratio. This implies the growth limitation for nanospindles. As the $[OH^-]/[Eu^{3+}]$ molar ratio increases to 300, there is slightly size change. The above experiments indicate that the size of the $Eu(OH)_3$ nanospindles could be tuned by simply changing the $[OH^-]/[Eu^{3+}]$ molar ratio of the precursor.

We also investigated the effects of reaction time on the products. As the reaction time was reduced to 10 min, the as-prepared samples are comprised of aggregates of amorphous particles and nanospindles (Fig. 7a). When the reaction time was increased to 1 h, the nanoparticles disappeared, and the size of nanospindles increases (Fig. 7b). It can be concluded that the nanoparticles are only an intermediate and will gradually form nanospindles with

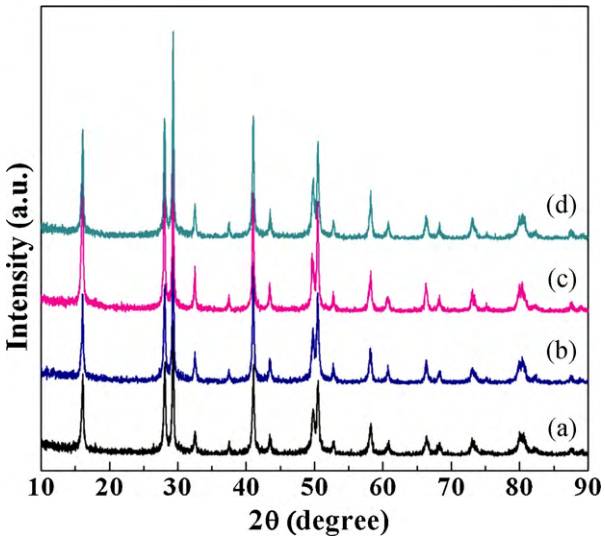


**Fig. 8.** XRD patterns of $Eu(OH)_3$ nanospindles prepared at R.T. for various aging times: (a) 2 h, (b) 6 h, (c) 36 h and (d) 72 h.

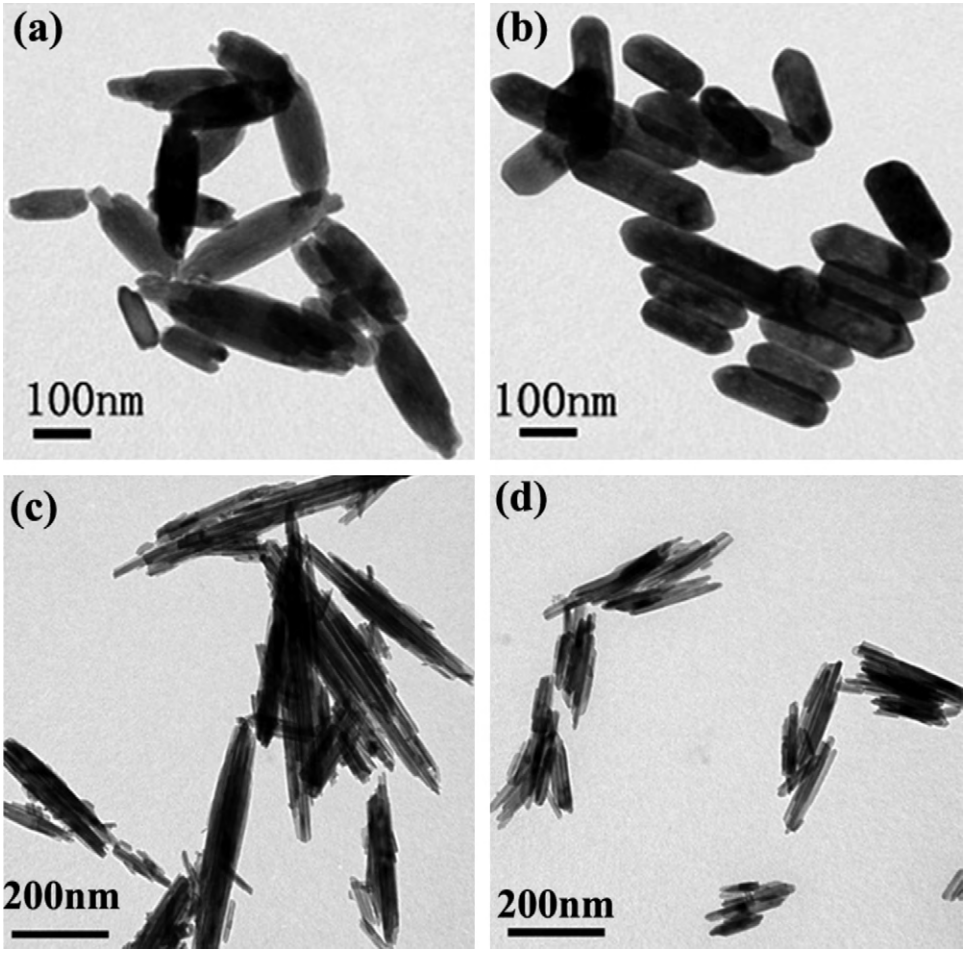


**Fig. 9.** TEM images of $Eu(OH)_3$ nanorods prepared with the $[OH^-]/[Eu^{3+}]$ molar ratio of 240 for 24 h at different temperatures: (a) 40 °C and (b) 80 °C; the $Eu(OH)_3$ nanobundles prepared with the $[OH^-]/[Eu^{3+}]$ molar ratio of 25 for 24 h at different temperatures: (c) 40 °C and (d) 80 °C.

increasing reaction time. The reaction time from 6 to 72 h has little influence on the morphology of $Eu(OH)_3$ nanospindles (Fig. 7c and d). But the diffraction peaks (Fig. 8) become sharper and stronger with increasing reaction time, which suggests that the longer reaction time can improve the crystallization of $Eu(OH)_3$ nanospindles.

To trace the growth process of the $Eu(OH)_3$ nanospindles, we have investigated the effects of temperature on the products. Fig. 9a and b shows the representative TEM images of as-prepared $Eu(OH)_3$ at the $[OH^-]/[Eu^{3+}]$ molar ratio of 240 and aged at 40 and 80 °C . It can be seen that the products are composed of shorter and thicker nanorods instead of the nanospindles. It is interesting to find that the end elevation of the nanorods reveals pyramid-like ends. However, the $Eu(OH)_3$ nanospindles have spin-like ends. The $Eu(OH)_3$ nanocrystals can easily fuse to each other by facets and grew as a whole, and then the $Eu(OH)_3$ nanorods formed [38]. Fig. 9c and d shows the representative TEM images of as-prepared $Eu(OH)_3$ at the $[OH^-]/[Eu^{3+}]$ molar ratio of 25 and aged at 40 and 80 °C. The morphology of the corresponding products is primarily large-scale nanobundles, which are made up of nanorods. Under low concentration and higher temperature condition, nanorods are firstly formed due to the hexagonal crystal structure, and then become attached to each other in an oriented fashion which results in the formation of nanobundles.

To investigate the role of vigorous agitation in the formation of the nanospindles, the control reaction employed without vigorous agitation is conducted with other conditions unchanged. The typical TEM images of the nanobundles are shown in Fig. 10. No regular nanospindles are obtained. But the irregular nanobundles coexist with some nanorods.

It is concluded that the vigorous agitation, temperature, and the $[OH^-]/[Eu^{3+}]$ molar ratio in the reaction system are the key factors for the formation of $Eu(OH)_3$ nanospindles. The optimum conditions of forming $Eu(OH)_3$ nanospindles are of lower temperature with vigorous agitation and higher the $[OH^-]/[Eu^{3+}]$ molar ratio.

Based on the above experimental results and analyses, it is proposed that the formation of $Eu(OH)_3$ nanospindles at R.T. can be suggested as follows. It is well known that the crystal growth and crystal morphology are controlled by the extrinsic and intrinsic factors, such as diffusion of the reaction, the degree of supersaturation, surface energy, crystal structure and etc. in the solution reaction system [39,40]. Two growth processes of the formation of $Eu(OH)_3$ nanospindles are involved: nucleation/growth of primary particles, and the aggregation growth process of the nanospindles by primary particles aggregation [25]. A large number of small nuclei are rapidly formed in the supersaturated solution at the beginning of the reaction because of the fast reaction between $Eu(NO_3)_3$ and NaOH aqueous solution. Nanospindles growth is at the expense of the primary particles. In our experiment, NaOH not only is a source of hydroxyl ions to form $Eu(OH)_3$ nanospindles, but also plays an important role similar to a capping agent for promoting $Eu(OH)_3$ nanospindles, which is the same as the formation of the brush-like ZnO hierarchical nanostructures reported by Zhang et al. [41]. The low $OH^-$ concentration has a small effect on the intrinsic growth habit of $Eu(OH)_3$. In general, materials with a hexagonal structure, the anisotropic growth along the c axis is available to form the 1D nanostructure, as the large polar surface is generally energetically unfavorable unless the surface charges are compensated by capping agents [42]. At a high $OH^-$ concentration, $OH^-$ ions are preferably adsorbed on the {0 0 1} and {1 0 0} plane of $Eu(OH)_3$ as compared with {1 1 0} crystal planes [43], resulting in different growth rates of different planes to form $Eu(OH)_3$ nanospindles. The absorbed $OH^-$ ions not only passivate the surface of nanocrystals but also prevent

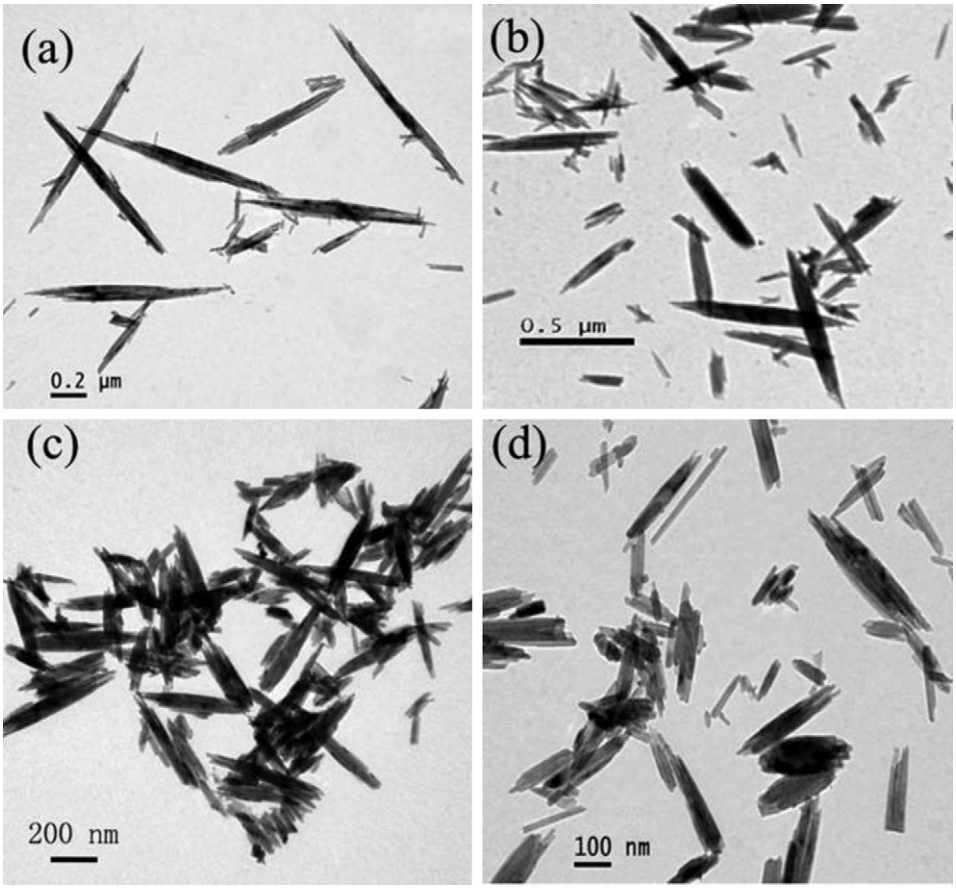


**Fig. 10.** TEM images of $Eu(OH)_3$ nanospindles prepared at R.T. without agitation under different $[OH^-]/[Eu^{3+}]$ molar ratios: (a) 25, (b) 50, (c) 250, and (d) 300.

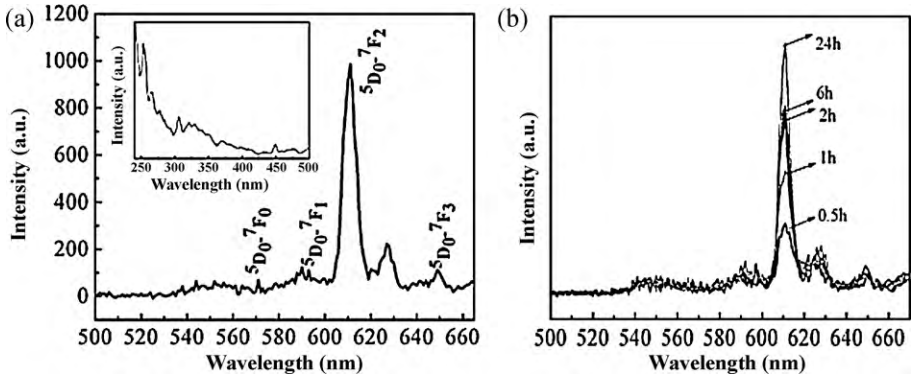


**Fig. 11.** (a) The room-temperature emission spectrum of $Eu_2O_3$ nanospindles (excitation at 254 nm). Corresponding excitation spectrum monitored at 611 nm emission is shown as an inset. (b) The emission spectrum of the as-prepared nanospindles aging for different times.

the agglomeration. So the uniform and monodisperse nanospindles are obtained. Earlier studies indicate that adsorbed ions can change the growth kinetics and the surface energies of different crystal faces, which can ultimately lead to anisotropic growth of low symmetry nanostructures [44]. When the capping ability of the $OH^-$ ions increase significantly with the increase of its amount, some $OH^-$ ions are adsorbed on the {1 1 0} crystal planes as a surface termination reagent, which suppresses the growth of crystal face {1 1 0}.

As the reaction temperature increases, $Eu(OH)_3$ nanorods are obtained (Fig. 9a and b) due to the decrease of the absorption force between $OH^-$ ions and the surface of $Eu(OH)_3$ nanoparticles. The

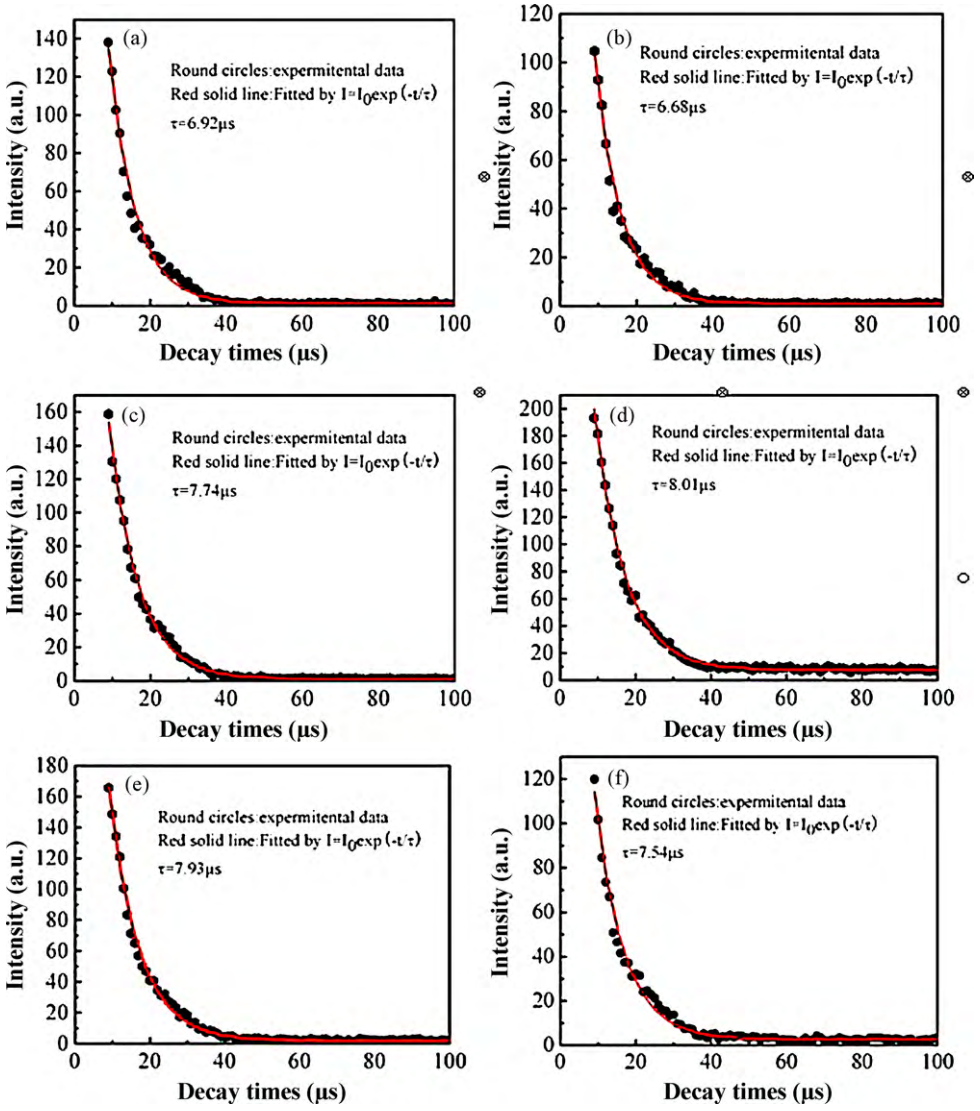


**Fig. 12.** Room-temperature decay curves of $Eu^{3+}$ luminescence (~611 nm) of $Eu_2O_3$ nanospindles prepared at various conditions recorded with fixed $\lambda_{ex}$ = ~263 nm and $\lambda_{ex}$ = ~611 nm: (a) R.T. for 2 h, (b) R.T. for 6 h, (c) R.T. for 24 h, (d) R.T. for 72 h, (e) 40 °C for 24 h, and (f) 80 °C for 24 h.

europium hydroxides have a strong tendency toward 1D growth along the [0 0 1] direction, so nanorods are formed.

In this investigation, such nanospindles are formed without the influence of any surfactant. Although the exact growth mechanism of the $Eu(OH)_3$ nanospindles is not very clear, we believe that NaOH plays an important role similar to the so-called soft template for promoting the anisotropic growth and their self-assemble to nanospindles. Rare earth metal hydroxides have a similar crystal structure. The spindle-like $Gd(OH)_3$ and $Sm(OH)_3$ were also synthesized in this method, as shown in Fig. 1S (supporting information). So this method might be extended to other rare earth metal hydroxides and oxides.

### 3.3. Photoluminescence property of $Eu_2O_3$ nanospindles

Fig. 11a (inset) shows the excitation spectra of $Eu_2O_3$ nanospindles at R.T. by monitoring the emission wavelength at 611 nm. Two sets of lines have been observed. The strong band at ~251 nm is assigned to the charge transfer transition between $O^{2-}$ and $Eu^{3+}$, which is related to the covalence between $O^{2-}$ and $Eu^{3+}$ and the coordination environment around $Eu^{3+}$ [45]. Other weaker bands are assigned to the direct excitation of the f–f shell transition of $Eu^{3+}$.

Fig. 11a shows the room-temperature emission spectra of $Eu_2O_3$ nanospindles. The sample is measured under an excitation wavelength of 254 nm. The emission peaks are composed of the characteristic emission lines of $Eu^{3+}$, corresponding to $^5D_0$–$^7F_J$ ($J$ = 0, 1, 2, 3). Among these emission peaks, the $^5D_0$–$^7F_2$ peak is dominant in comparison with any other peaks, which is a hypersensitive forced electric dipole transition [46]. It is known that the f–f transition arising from a forced electric dipole is forbidden but becomes partially allowed when the rare earth ion is situated at a low symmetry site [47].

Fig. 11b shows the photoluminescence spectra of the nanospindles aging for different times. The relative peak intensity increases as the reaction time increased. As can be seen from XRD patterns that the diffraction peaks (Fig. 8) become sharper and stronger with increasing the reaction time. It is suggested that the high crystallinity may improve the photoluminescence intensity, which is similar to the previous reports [17,35,48]. Wang et al. reported that a high degree of crystallinity and a larger crystallite are considered to be the reason for improved photoluminescence intensity [48]. Similarly, Zhang et al. reported that the emission intensity of $YF_3$:Eu nanospindles increases when the reaction time was increased [5].

Fig. 12 shows the room-temperature decay curves of $Eu^{3+}$ luminescence (~611 nm) of $Eu_2O_3$ nanospindles prepared at various conditions. These decay curves can be well fitted by a single exponential function as $I = I_0 \exp(-t/\tau)$, where $I_0$ is the initial emission intensity at $t = 0$ and $\tau$ is the $1/e$ lifetime of the emission center. The lifetime of $Eu_2O_3$ nanospindles prepared at various aging temperatures and times is as follows: 6.92 μs (R.T. for 2 h), 6.68 μs (R.T. for 6 h), 7.74 μs ((R.T. for 24 h), 8.01 μs ((R.T. for 72 h), 7.93 μs (40 °C for 24 h), and 7.54 μs (80 °C for 24 h). The lifetime of those samples is quite close in the same microsecond scale, which is much shorter than that of Eu-doped systems. The short lifetime is due to high $Eu^{3+}$ concentration in which the non-radiative mechanisms govern the processes [49]. This result indicates that the reaction temperature and time affecting the photoluminescence intensity have little effect on the lifetime of the samples.

## 4. Conclusions

In summary, the uniform and single-crystalline $Eu(OH)_3$ with different morphologies have been successfully prepared in high yield by a liquid deposition method. Our results show that a soft chemical route is promising for rational and structural design of nanostructured materials. The R.T. photoluminescence analysis shows that $Eu_2O_3$ nanostructures have a strong red emission peak of $Eu^{3+}$ ion at around 611 nm due to the $^5D_0$–$^7F_2$ forced electric dipole transition of $Eu^{3+}$ ions. It is believed that these $Eu_2O_3$ nanospindles, nanorods and nanobundles possess the potential and diverse applications, such as laser materials, phosphors, field emitters, and nanometer-scale optoelectronic devices.

## Acknowledgments

The authors acknowledge the supports of Natural Science Foundation of Shanghai (08ZR1407600), Shanghai Rising-Star Program (10QA1402400), Shanghai Educational Development Foundation (2008CG49), Innovation Program of Shanghai Municipal Education Commission (09YZ18), and Leading Academic Discipline Project of Shanghai Municipal Education Commission (J50102). The authors would like to thank Mr. Y.L. Chu and Mr. W.J. Yu for help with the SEM and TEM measurements.

## Appendix A. Supplementary data

Supplementary data associated with this article can be found, in the online version, at doi:10.1016/j.jallcom.2010.07.026.

## References

[1] L.J. Lauhon, M.S. Gudiksen, C.L. Wang, C.M. Lieber, Nature 420 (2002) 57.
[2] Y. Zhang, Q. Xiang, J.Q. Xu, P.C. Xu, Q.Y. Pan, F. Li, J. Mater. Chem. 19 (2009) 4701.
[3] Z.G. Yan, C.H. Yan, J. Mater. Chem. 18 (2008) 5046.
[4] J.P. Liu, X.T. Huang, K.M. Sulieman, F.L. Sun, X. He, J. Phys. Chem. B 110 (2006) 10612.
[5] M.F. Zhang, H. Fan, B.J. Xi, X.Y. Wang, C. Dong, Y.T. Qian, J. Phys. Chem. C 111 (2007) 6652.
[6] Z.L. Wang, J.H. Song, Science 312 (2006) 242.
[7] H.P. Yang, D.S. Zhang, L.Y. Shi, J.H. Fang, Acta Mater. 56 (2008) 955.
[8] C.R. Patra, R. Bhattacharya, S. Patra, N.E. Vlahakis, A. Gabashvili, Y. Koltypin, A. Gedanken, P. Mukherjee, D. Mukhopadhyay, Adv. Mater. 20 (2008) 753.
[9] K.L. Wong, G.L. Law, M.B. Murphy, P.A. Tanner, W.T. Wong, P.K.S. Lam, M.H.W. Lam, Inorg. Chem. 47 (2008) 5190.
[10] M. Vasile, P. Vlazan, N.M. Avram, J. Alloys Compd. 500 (2010) 185.
[11] X.R. Hou, S.M. Zhou, Y.K. Li, W.J. Li, J. Alloys Compd. 494 (2010) 382.
[12] A. Gulino, F. Lupo, G.C. Condorelli, A. Motta, I.L. Fragalà, J. Mater. Chem. 19 (2009) 3507.
[13] W.Q. Fan, S.Y. Song, J. Feng, Y.Q. Lei, G.L. Zheng, H.J. Zhang, J. Phys. Chem. C 112 (2008) 19939.
[14] K.M. Nissamudeen, K.G. Gopchandran, J. Alloys Compd. 490 (2010) 399.
[15] X. Bai, H.W. Song, L.X. Yu, L.M. Yang, Z.X. Liu, G.H. Pan, S.Z. Lu, X.G. Ren, Y.Q. Lei, L.B. Fan, J. Phys. Chem. B 109 (2005) 15236.
[16] C.T. Lee, F.S. Chen, C.H. Lu, J. Alloys Compd. 490 (2010) 407.
[17] T.T. Yan, D.S. Zhang, L.Y. Shi, H.P. Yang, H.L. Mai, J.H. Fang, Mater. Chem. Phys. 117 (2009) 234.
[18] X.C. Song, E. Yang, R. Ma, H.F. Chen, Z.L. Ye, M. Luo, Appl. Phys. A 94 (2009) 185.
[19] V.G. Pol, O. Palchik, A. Gedanken, I. Felner, J. Phys. Chem. B 106 (2002) 9737.
[20] N. Du, H. Zhang, B.D. Chen, J.B. Wu, D.S. Li, D.R. Yang, Nanotechnology 18 (2007) 065605.
[21] X. Wang, Y.D. Li, Angew. Chem. Int. Ed. 41 (2002) 4790.
[22] G.S. Wu, L.D. Zhang, B.C. Cheng, T. Xie, X.Y. Yuan, J. Am. Chem. Soc. 126 (2004) 5976.
[23] M. Pumera, M. Cabala, K. Veltruska, I. Ichinose, J. Tang, Chem. Mater. 19 (2007) 6513.
[24] L.X. Zhang, J. Luo, M.Z. Wu, H.F. Jiu, Q.W. Chen, Mater. Lett. 61 (2007) 4452.
[25] S.F. Wang, F. Gu, C.Z. Li, M.K. Lv, Cryst. Growth Des. 7 (2007) 2670.
[26] Z.H. Xu, C.X. Li, P.P. Yang, Z.Y. Hou, C.M. Zhang, J. Lin, Cryst. Growth Des. 9 (2009) 4127.
[27] J. Geng, J.J. Zhu, D.J. Lu, H.Y. Chen, Inorg. Chem. 45 (2006) 8403.
[28] C.C. Yu, M. Yu, C.X. Li, C.M. Zhang, P.P. Yang, J. Lin, Cryst. Growth Des. 9 (2009) 783.
[29] P. Liu, C.X. Wang, X.Y. Chen, G.W. Yang, J. Phys. Chem. C 112 (2008) 13450.
[30] F. Li, M. Wang, C.C. Mi, K.Y. Yi, S.K. Xu, J. Alloys Compd. 486 (2009) L37.
[31] W.B. Bu, L.X. Zhang, Z.L. Hua, H.R. Chen, J.L. Shi, Cryst. Growth Des. 7 (2007) 2305.
[32] H.S. Qian, P. Gunawan, Y.X. Zhang, G.F. Lin, J.W. Zheng, R. Xu, Cryst. Growth Des. 8 (2008) 1282.
[33] X. Peng, Chem. Eur. J. 8 (2002) 334.
[34] D.S. Zhang, X.Q. He, H.P. Yang, L.Y. Shi, J.H. Fang, Appl. Surf. Sci. 255 (2009) 8270.
[35] T.T. Yan, D.S. Zhang, L.Y. Shi, H.R. Li, J. Alloys Compd. 487 (2009) 483.
[36] C. Tang, Y. Bando, B. Liu, D. Golberg, Adv. Mater. 17 (2005) 3005.

[37] Z.P. Zhang, H.P. Sun, X.Q. Shao, D.F. Li, H.D. Yu, M.Y. Han, Adv. Mater. 17 (2005) 42.
[38] T. Maddanimath, A. Kumar, J. D'Arcy-Gall, P.G. Ganesan, K. Vijayamohanan, G. Ramanath, Chem. Commun. 11 (2005) 1435.
[39] M.J. Siegfried, K.S. Choi, Adv. Mater. 16 (2004) 174.
[40] L. Zhen, W.S. Wang, C.Y. Xu, W.Z. Shao, L.C. Qin, Mater. Lett 62 (2008) 1740.
[41] Y. Zhang, J.Q. Xu, Q. Xiang, H. Li, Q.Y. Pan, P.C. Xu, J. Phys. Chem. C 113 (2009) 3430.
[42] B.Q. Cao, W.P. Cai, J. Phys. Chem. C 112 (2008) 680.
[43] L. Zhu, J. Meng, X.Q. Cao, Eur. J. Inorg. Chem. (2007) 3863.
[44] K.K. Caswell, C.M. Bender, C.J. Murphy, Nano Lett. 3 (2003) 667.
[45] H.E. Hoefdraad, J. Solid State Chem. 15 (1975) 175.
[46] R. Bazzi, M.A. Flores, C. Louis, K. Lebbou, W. Zhang, C. Dujardin, S. Roux, B. Mercier, G. Ledoux, E. Bernstein, P. Perriat, O. Tillement, J. Colloid Interface Sci. 273 (2004) 191.
[47] A. Patra, E. Sominska, S. Ramesh, Y. Koltypin, Z. Zhong, H. Minti, R. Reisfeld, A. Gedanken, J. Phys. Chem. B 103 (1999) 3361.
[48] W.N. Wang, W. Widiyastuti, T. Ogi, I.W. Lenggoro, K. Okuyama, Chem. Mater. 19 (2007) 1723.
[49] Y. Castro, B. Julian, C. Boissière, B. Viana, H. Amenitsch, D. Grosso, C. Sanchez, Nanotechnology 18 (2007) 055705.